Typical phases of pre-failure damage in granitic rocks under differential compression

XINGLIN LEI[1]

Institute of Geology and Geoinformation/GSJ, National Institute of Advanced Industrial Science and Technology (AIST), Higashi 1-1-1, AIST no. 7, Tsukuba 305-8567, Japan (e-mail: xinglin-lei@aist.go.jp)

[1]*Also at State Key Laboratory of Earthquake Dynamics, Institute of Geology, Chinese Earthquake Administration, Beijing, China*

Abstract: The evolution of pre-failure damage in brittle rock samples subjected to differential compression has been investigated by means of acoustic emission (AE) records. The experimental results show that the damaging process is characterized by three typical phases of microcracking activity: primary, secondary, and nucleation. The primary phase reflects the initial activity of pre-existing microcracks, and is characterized by an increase, with increasing stress, both in event rate and *b* value. The secondary phase involves subcritical growth of the microcrack population, revealed by an event rate increase and a dramatic decrease of the *b* value. The nucleation phase corresponds to initiation and accelerated growth of the ultimate macroscopic fracture along one or more incipient fracture planes. During the nucleation phase, the *b* value decreases rapidly to the global minimum value around 0.5. The temporal variation of *b* in every phase clearly correlates with grain size of the test sample, hence indicating that a comparatively larger grain size results in a lower *b* value. In order to investigate the fracture mechanism of each phase, a damage model was tested by employing the constitutive laws of subcritical crack growth of crack populations with a fractal size distribution.

Abundant experimental evidence shows that macroscopic shear failure in rock does not occur by the growth of a single crack in its own plane. Rather, shear failures are preceded by a complex evolution of some pre-failure damage (Lockner *et al.* 1991; Lei *et al.* 2004). Therefore, studies focusing on both fracture dynamics and pre-failure damage are a subject of widespread interest, having relevance for several applications, such as safe design of deep tunnelling (e.g. Diederichs *et al.* 2004), and natural processes such as volcanism and seismology (e.g. Ponomarev *et al.* 1997; Diodati *et al.* 2000). The fracturing dynamics and damage evolution in stressed materials has been extensively studied in the laboratory by a number of methods, including (1) direct observation of samples by scanning electron microscopy (e.g. Zhao 1998) or optical microscopy (Cox & Scholz 1988) operated during or after a fracture test and (2) monitoring of the space distribution of acoustic emission (AE) events caused by microcracking (e.g. Lockner *et al.* 1991; Lei *et al.* 1992). The fracturing dynamics and the pre-failure damage can be inferred from AE statistics, as the number of AE events that is proportional to the number of growing cracks, and the AE amplitudes are both proportional to the length of crack growth increments in the rock (e.g. Main *et al.* 1989, 1993; Sun *et al.* 1991). Therefore, the AE technique is applied to the analysis of the microcracking activity inside the sample volume, and it can be performed under confining pressure, which is very important for the simulation of underground conditions. In addition, owing to the mechanical and statistical similarities between AE events and earthquakes, AE in rocks is studied as a model of natural earthquakes (Ponomarev *et al.* 1997). The disadvantage of the AE technique is that it is insensitive to ductile deformation, which does not produce appreciable AE. Therefore, it is applicable only in brittle regimes.

The recently developed high-speed, multichannel waveform recording technology permitted monitoring with high precision of the AE events associated with spontaneously/unstably fracturing processes within stressed samples. It was applied to the analysis of the fracture process of hornblende schist (Lei *et al.* 2000*b*), of two granitic rocks of extremely different density with a pre-existing microcrack (Lei *et al.* 2000*a*), and mudstone containing quartz veins resembling strong asperities (Lei *et al.* 2000*c*). The above studies show that the fracturing of several samples containing faults of widely differing strength exhibit three long-term microcracking phases: primary, secondary, and nucleation (Lei *et al.* 2004), and that the

From: CELLO, G. & MALAMUD, B. D. (eds) 2006. *Fractal Analysis for Natural Hazards.* Geological Society, London, Special Publications, **261**, 11–29.
0305-8719/06/$15.00

density of pre-existing cracks is a major controlling factor in the fracture and pre-failure damage evolution of rocks (Lei *et al.* 2000*a*). Besides crack density, the size distribution of pre-existing cracks is another important factor. Following Tapponier & Brace (1976) we assume that the size distribution of pre-existing cracks is consistent with the grain size distribution in each test sample; in other words, we assume that samples of comparatively larger grain size have a larger number of cracks of larger sizes. In order to check this assumption and identify the typical phases during pre-failure damage, systematic experiments were carried out at different loading rates on granites of different grain size distributions (Lei *et al.* 2005).

One major purpose of a study on pre-failure damage is to consider the possibility of predicting the time of the catastrophic failure event from damage evolution. The ever-increasing interest in such predictions is associated with damage models based either on statistics of critical phenomena or on the experimental knowledge about subcritical crack growth. It is well known that subcritical crack growth under stress can be considered a result of stress-aided corrosion at the crack tip. Owing to this, some fracture laws were proposed based on the experimental results of a single macroscopic extensional crack (e.g. Das & Scholz 1981; Meredith & Atkinson 1983). They were later extended to crack populations whose size distribution is fractal (e.g. Main *et al.* 1993). These types of models predict not only the event release rate, but also the seismic *b* value (the exponent of the power-law magnitude–frequency relation) (Lei *et al.* 2005); in addition, they may explain some precursory anomalies, such as quiescence (Main & Meredith 1991) and *b* value decrease (Main *et al.* 1989) associated with large earthquakes.

The present paper aims on the one hand to confirm the typical phases of pre-failure damage, and on the other hand, to improve available damage models. For this purpose, AE data obtained from a series of experiments are here analysed and summarized. Experimental data obtained under a constant stress-rate loading (including some creep tests) on samples of several granitic lithologies were used for summarizing the typical common features of pre-failure damage. Such samples were selected in order to check the roles, for the fracturing behaviour, of grain size, of the pre-existing microcrack density, and of macroscopic structures such as healed joints. The first two sections focus on a review of the experimental and data-processing procedures. Typical experimental results are summarized in the third section; then, an improved model is evaluated. Finally, some plausible physical mechanisms occurring during every damage phase are discussed.

Experimental procedure

Rock samples

Table 1 lists the analysed lithologies and their mechanical properties, including grain size, density of pre-existing crack, and the minimum/maximum P-velocities (V_{min}, V_{max}) along the axial direction. Because most pre-existing cracks are likely to be closed following stress increase, the difference $V_{max} - V_{min}$ can be considered as a qualitative measurement of pre-existing microcrack density. Some samples contain one or more veins (healed joints), which evolved during compression into the ultimate fracture plane. The size and spatial distribution of pre-existing microcracks are controlled by the grain size distribution (Tapponier & Brace 1976); hence, on the scale range from microcrack size to sample dimension, rocks of larger grain size generally respond more heterogeneously during the fracturing process. The Westerly granite (WG) is fine-grained and has the smallest grain size. The Inada granite (IG), the Tsukuba granite (TG), the Mayet granite (MG) and the granitic

Table 1. *Some mechanical properties of the test samples*

Rock type	Grain size (mm) range/major	Density of pre-existing cracks	Axial V_p (km s^{-1}) min/max
Westerly granite (WG)	<2/<1	High	4.8/5.6
Oshima granite (OG)	1–5/~2	High	4.4/5.8
Inada granite (IG)	1–10/~7	High	4.2/5.8
Granitic porphyry (GP)	1–10/~6	Very low	5.8/6.0
Tsukuba granite (TG)	1–30/~10	High	4.2/5.8
Mayet granite (MG)	1–30/~15	Low	5.2/6.1
S-C cataclasite (SC)	1–10/~5	Very high	4.2/5.6
Nojima granite (NG)	1–10/~5	High	4.7/5.7

porphyry (GP) are typical coarse-grained lithologies. The Oshima granite (OG) is classified into intermediate-grained rock, and has a mean grain size greater than WG but smaller than IG. Consistent with the value of $V_{max} - V_{min}$, the density of pre-existing cracks is high in WG, OG, IG, and TG, whereas it is relatively low in MG, and GP is almost crack-free (Lei *et al.* 2000*a*).

The WG, OG, and IG are suited for investigating the role of grain size on fracture behaviour, because they have similar mineralogical content and density of pre-existing microcracks, contrasting with significantly different grain size distribution. The MG and TG samples were selected for checking the role of heterogeneity at large scales either because they contained some large grains or because they contained healed joints. A foliated granitic cataclasite (CG) and its host Nojima granite (NG) were also used, in order to investigate the fracture behaviour of such weak rock in or near a fault zone. The SC and NG samples were collected from drill cores on the Nojima active fault zone at a depth of ~200 m. The Nojima fault, located in southwest Japan, ruptured in the 1995 Kobe earthquake (Lin 2001). The experimental results obtained from the MG samples were preliminarily presented by Jouniaux *et al.* (2001). In the present study, the hypocentre of every AE event was redetermined after checking every arrival time. Such hard work greatly improved the precision of the hypocentres.

The test samples were shaped into cylinders of 125 mm or 100 mm length and 50 mm diameter. All samples were dried under normal room conditions for more than one month and then they were compressed at a constant stress rate or at a constant stress (creep test) at a stress level of ~95% the nominal fracture strength at room temperature (air-conditioned at ~25°C). During the deformation, the confining pressure was maintained at a constant level of 40 or 60 MPa within the brittle regime. Under these conditions, the rock samples normally fractured along a compression shear fault oriented at ~30° with respect to the axis of maximum compressive stress.

Experimental apparatus

Figure 1 shows the functional block diagram of the experimental set-up along with important details of the loading apparatus, AE recorder, and other data acquisition systems. The assembled pressure vessel was placed in a loading frame and high-pressure fluid lines attached for external confining pressure. Hydraulic oil was used for the confining pressure medium. As many as 32 PZTs (piezoelectric transducers, compressional mode, 2 MHz resonant frequency, 5 mm in diameter) were mounted on the sample surface for detecting the AE signals produced by microcracking events. The signal is pre-amplified by 40 dB before feeding into the high-speed waveform recording system, which has a maximum sampling rate of 40 ns and a dynamic range of 12 bits. Two peak detectors were used to capture the values of the maximum amplitudes, from two artificially selected sensors, after 20 or 40 dB pre-amplifiers. An automatic switching subsystem was designed for sequentially connecting every selected sensor, in total as many as 18, to the pulse generator for velocity measurement. Such a high-speed AE monitoring system can record the maximum amplitude and waveform of the AE signals with no major loss of events, even for AE event rates of the order of several thousand events per second such as are normally observed before a catastrophic failure.

The AE hypocentres were determined by using the arrival times of the P wave and the measured P-velocities during every test. Location errors are generally less than 1–2 mm for fine-grained rocks and slightly greater for coarse-grained rocks. During every such test, the trigger threshold for waveform recording is about 10 times larger than the threshold for peak detection (i.e. for the detection of the maximum amplitude of the AE signal). In addition, at least four precise P arrival times are required for hypocentre determination. As a result, the hypocentre data are a subset of magnitude data. Besides AE measurement, eight 16-channel, cross-type strain gauges were mounted on the surface of the test samples for measuring the local strains along the axial and circumferential directions. Stress, strain, and confining pressure were digitized at a resolution of 16 bits and sampling interval of millisecond order. The local volumetric strain (ϵ_v) was calculated from the axial (ϵ_a) and circumferential (ϵ_c) strains according to the equation $\epsilon_v = \epsilon_a + 2\epsilon_c$. The mean strains of the test sample were estimated by averaging these local measurements.

Data processing

The statistical parameters which better characterize the pre-failure damaging behaviours are

(1) energy release rate and cumulative energy release including event rate and cumulative number;
(2) b value in the frequency–magnitude distribution; and
(3) fractal dimension of the AE hypocentre.

In the following sections it will be briefly illustrated how the above parameters were estimated.

Normalized time-to-failure

Rock fracturing is generally characterized as a fast transient phenomenon showing a high degree of

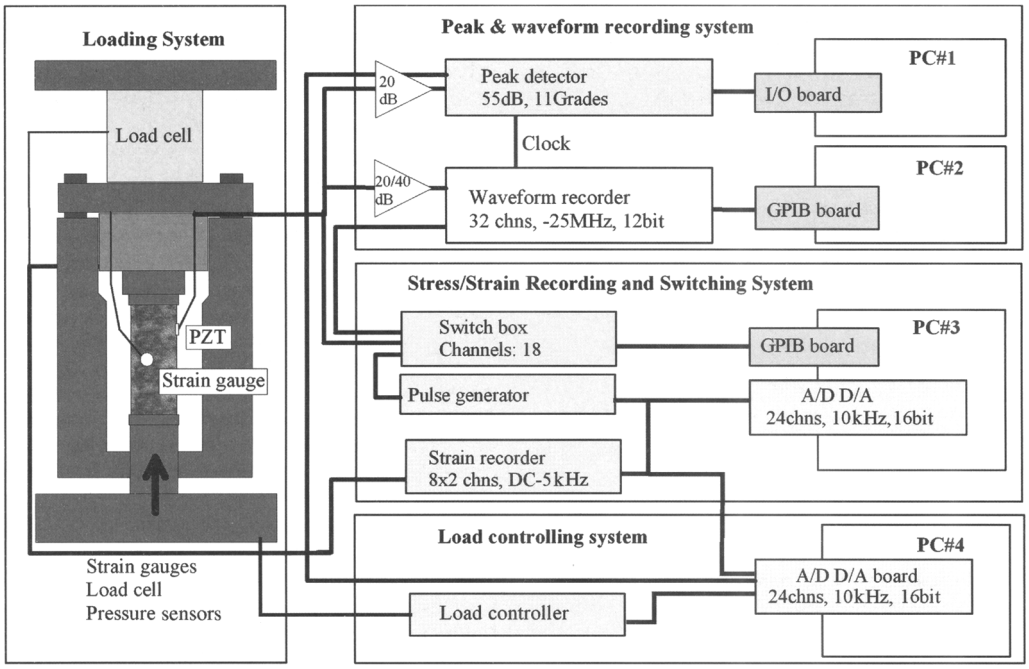

Fig. 1. Block diagram of the experimental apparatus used for rock fracture tests. Up to 32 PZT sensors were mounted on the surface of the test sample (a rock cylinder of 125 mm length and 50 mm diameter). The signal is pre-amplified by 40 dB before feeding into the high-speed waveform recording system, which has a maximum sampling rate of 40 ns and a dynamic range of 12 bits. Two peak detectors were used to capture the values of the maximum amplitudes, from two artificially selected sensors, after 20 or 40 dB pre-amplifiers. An automatic switching subsystem was designed for sequentially connecting every selected sensor, in total 18, to the pulse generator for velocity measurement. Stress, strain, and confining pressure were digitized at a resolution of 16 bits and sampling interval of millisecond order.

nonlinearity before the final failure. Plots of AE data v. time-to-failure in logarithmic scale are therefore helpful for presenting the details of the damaging process. The normalized time-to-failure is defined by:

$$\tilde{t} = \frac{t_f - t}{t_f - t_0} \quad (1)$$

where t_f is the failure time, t_0 is an artificial starting time that can be set, for example, as the onset time of AE activity or any other chosen time. In the present study, for modelling convenience, t_0 was set as the time of the maximum b value. These time instants correspond to the phase change from an initial rupture to subcritical crack growth of the crack population. This is discussed in detail in later sections.

AE magnitude and energy release rate

Following the definition of the body-wave earthquake magnitude, the magnitude (M) of an AE event is determined according to the log of the maximum amplitude (V_{max}) of the AE signal, as it represents the vibration velocity of the elastic wave (Lei *et al.* 2003), $M \propto \log V_{max} = A_{dB}/20$; here A_{dB} is the maximum amplitude in dB. Such definition results in magnitudes consistent with earthquake magnitudes. However, because the calibration parameter of the PZT sensor is unknown, the magnitudes that were obtained ought to be considered only as relative values. The amplitude threshold for the AE signals was set at 45 dB. Hence the AE magnitude was actually calculated using $M = (A_{dB} - 45)/20$. We note that the dynamic range of the system is 100 dB. As a result, every event with maximum amplitude equal to, or larger than, 100 dB would be recorded as $M = 2.75$. However, such saturation could be easily corrected by using the continuation time of the AE signal (Lei 2003). It should be noted that the maximum amplitude was digitized with 11 digits. The distinguishable magnitude interval is therefore 0.25.

The AE event rate $N = dn/dt$ gives the simplest measurement of the frequency of microcracking activity. The event rate can be calculated for

either a fixed number of events (dn) or a fixed time interval (dt). The two methods give similar results but may include different details. The generalized energy release correlates with magnitude:

$$E_i \propto 10^{CM_i} \tag{2}$$

where C is a constant. The most important cases are $C = 0.75$ and 1.5, which correspond to the Benioff strain and the classic energy release, respectively. The energy release rate can be estimated by summing Eq. (2) within a given unit time interval:

$$E = \sum_i 10^{CM_i}. \tag{3}$$

The cumulative energy release is simply defined by

$$\sum E = \int E\,dt. \tag{4}$$

The cumulative event number $\sum N$ can be considered as a special case of Eq. (4) with $C = 0$.

The b *value and recurrence time*

The Gutenberg–Richter relationship for magnitude–frequency distributions holds both for earthquakes and for AE events in rock samples (Scholz 1968; Liakopovlou-Morris *et al.* 1994). The cumulative number (N_m) of events with magnitude M or greater is a function of the magnitude (Gutenberg & Richter 1944):

$$\log_{10} N_m = a - bM. \tag{5}$$

In Eq. (5), a and b are constant; an estimate of the b value can be obtained by using either the least-squares method or the maximum likelihood method (Aki 1965; Utsu 1965; Bender 1983). For given n events, the latter method gives

$$\hat{b} = \frac{n \log_{10} e}{\sum_{i=1}^{n} (M_i - M_c + \Delta M/2)} = \frac{\log_{10} e}{\overline{M} - M_c + \Delta M/2} \tag{6}$$

where M_c is the cutoff magnitude and ΔM is the difference between successive magnitude units, which is 0.25 for the AE data. The approximate standard error of the b value estimate is $\hat{\sigma} = b/\sqrt{n}$ (Aki 1965), and the confidence limit of the estimation is given by

$$\sigma(b) = 2.30b^2 \Big/ \sqrt{\sum_{i=1}^{n} (M_i - \overline{M})^2/(n(n-1))} \tag{7}$$

where $\overline{M}$ denotes the mean magnitude estimation (Shi & Bolt 1982). In the present paper, the b values were sequentially calculated for consecutive groups of 500 to 8000 events ($n = 500$–8000) with an increment of $n/4$ events. A larger number of events leads to comparatively smoother curves, and it can be used for investigating the long-term trend. In contrast, a smaller number of events leads to a larger scatter, which reflects the complexity of the damage evolution. In the present paper, b_{LS} and b_{MLH} (or b) are used to denote the least-square b value and the maximum likelihood b value, respectively. In most experimental studies, the b value was calculated from the signals recorded by one AE sensor. Therefore, the focal distance from the source should be corrected for the attenuation. Nevertheless, the theoretical study by Weiss (1997) has shown that attenuation has no significant effect on the b value. In the present study, the signals from two sensors, mounted at different positions on the sample surface, were fed to peak detectors for recording the maximum amplitude. It was thus found that two sets of amplitude data result in consistent b values, although there are certain differences in the short-term fluctuations (Fig. 2).

On the basis of the a and b values, the probabilistic recurrence time T_r for an event with magnitude equal to, or greater than, a chosen M is estimated by

$$T_r = \Delta T/10^{a-bM}. \tag{8}$$

Here ΔT denotes the time length for which the a and b values are derived. In the present paper T_r was

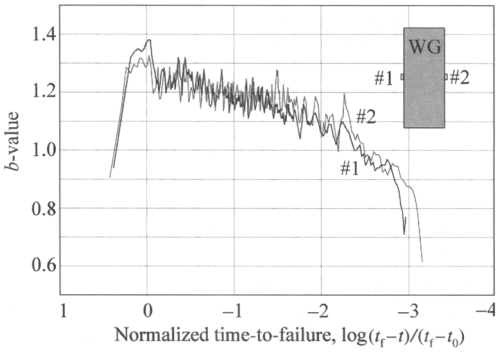

Fig. 2. Maximum likelihood b values calculated from AE signals obtained from two sensors (#1 – solid black line, #2 – solid grey line) are given as a function of the log of the normalized time-to-failure. The b values were sequentially calculated for consecutive data sets of 1000 events with an increment of 250 events. Also shown (grey rectangle in upper right) are the positions of AE sensors #1 and #2 with respect to the WG sample.

calculated for the maximum distinguishable magnitude of 2.75.

Fractal dimension of hypocentre distribution

A multifractal analysis was applied to the hypocentre distribution of AE events in order to examine quantitatively the spatial clustering of pre-failure damage. The multifractal concept is a natural extension of the (mono) fractal concept to the case of heterogeneous fractals. It was observed that the AE hypocentres, particularly in coarse-grained rocks, show heterogeneous fractal characteristics (Lei *et al.* 1993). In the present study, the generalized correlation-integral (Kurths & Herzel 1987), defined by the following equation, was used:

$$C_q(r) = \frac{1}{n}\left[\sum_{j=1}^{n}\left(\frac{n_j(R \le r)}{n-1}\right)^{q-1}\right]^{1/(q-1)} \quad (9)$$

$$(q = -\infty, \ldots, -2, -1, 0, 1, 2, \ldots, \infty)$$

where $n_j(R < r)$ is the number of hypocentre pairs separated by a distance equal to, or less than, r, q is an integer, and n is the total number of AE events analysed. If the hypocentre distribution exhibits a power law for any q, $C_q(r) \propto D_q$, the hypocentre population can be considered as a multifractal, and D_q defines the fractal dimension that can be determined by the least-squares fit on a log–log plot. In the case of a homogeneous fractal, D_q does not vary with q. However, in the case of a heterogeneous fractal, D_q decreases with increasing q and it is called the spectrum of the fractal dimension. It can be easily proved that D_0, D_1, and D_2 coincide with the information dimension, with the capacity dimension, and with the correlation dimension, respectively. The difference between D_2 and D_∞ is an index representing the degree of heterogeneity of the fractal set. Normally, D_{20} is an efficiently precise estimation of D_∞.

Fractal analysis was applied routinely either for every group of 100–200 hypocentres, or for every group of 2000–8000 events, in order to inspect the temporal evolution of the fractal structure and the correlation between fractal dimension and b value. For the later case, that is, with a fixed number of events, as mentioned in the previous section, the hypocentre data are a subset of the magnitude data. The average actual number of hypocentres, which were precisely determined and were thus available for fractal analysis in every group, is normally in the order of several hundreds. The minimum number of hypocentres required for applying fractal analysis was artificially set as 100 for determining reliable D values. The fractal dimension of every group with a number of hypocentres less than 100 was not determined.

Experimental results

Systematic experiments on granitic rock samples were performed at different loading rates, in order to investigate the statistical behaviour of pre-failure damage and to set an appropriate damage model. A large number of AE events, from tens to hundreds of thousand, were observed during every test. As an example, Figure 3 shows the AE record of a typical test of IG sample subjected to a constant loading rate at 27.5 MPa min^{-1}. As may be seen, the AE data, particularly the energy release rate and the b value, exhibit some typical phases of pre-failure damage, (see also Lei *et al.* 2003, 2004) and microcracking activity initiated at a stress level of ~35% of the sample's fracture strength. The event rate generally increases, with increasing stress, up to the failure point. Following Lei *et al.* (2003, 2004), in the following sections, a three-phase model including a primary, a secondary, and a nucleation phase, will be used for describing such behaviour.

The AE data obtained from the IG, OG, and WG samples are partly summarized in Figure 4, where it is clearly shown that the three distinct phases are a universal feature during rock fracture in the brittle domain. The common features of each phase are summarized in the following sections.

Primary phase

During this phase, microcracking activity was initiated at stress levels of 30–60% of fracture strength of every sample. Such stress values strongly depend on the density and size distribution of pre-existing cracks, and such distributions are controlled by the grain-governed heterogeneity within the sample. In general, a lithology with comparatively larger mean grain sizes or with higher pre-existing microcrack density exhibits a lower initiation stress and a higher AE activity. During the primary phase, the event rate is low and it increases slightly with the increase of stress or time. The b value increases, with increasing stress, from an initial value of 0.5–1.2 to 1.0–1.4. The initial and final values also depend on the density and size distribution of the pre-existing microcracks. In the fine-grained WG, the primary phase is not clearly distinguishable, involving only a small number of events, with a high

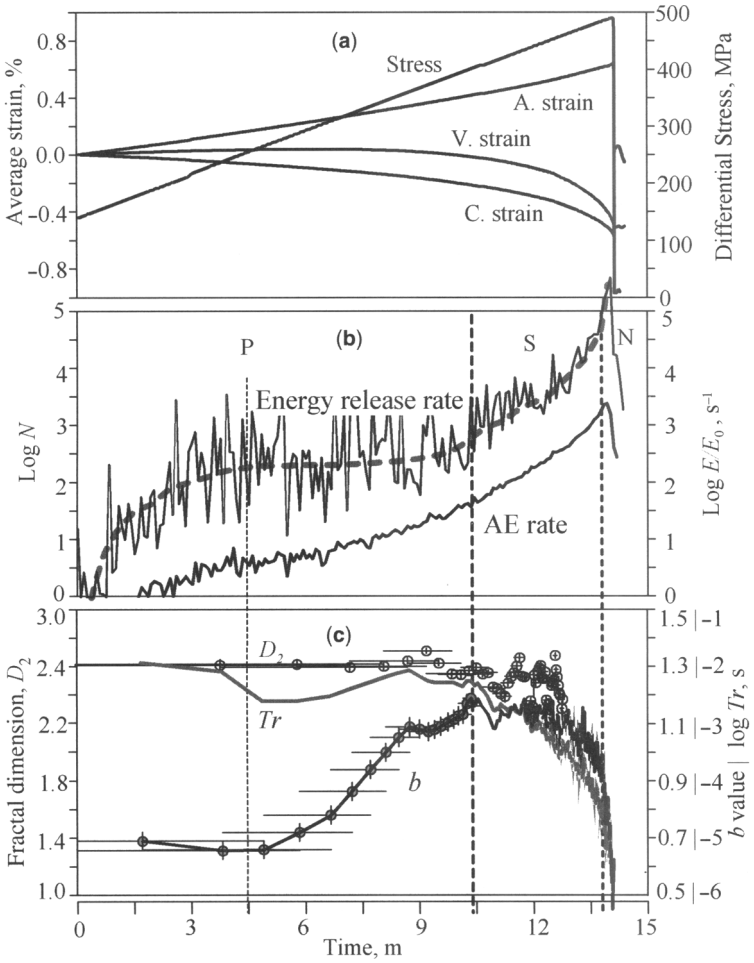

Fig. 3. An example of AE data obtained from a typical experiment on an IG sample. (**a**) Differential stress, average axial/circumferential/volumetric strains v. time. (**b**) AE energy release rate and event rate calculated consecutively for every 10 s. (**c**) *b* Value, recurrence time (T_r) value and fractal dimension (D_2) v. time. P, S, and N in (**b**) denote the primary, secondary and nucleation phases, respectively. The time interval and standard error for all *b* and D_2 data are shown by the horizontal and vertical bars, respectively.

initial *b* value and a small increase (from ~1.2 to ~1.4, Fig. 4e, f). In contrast, the primary phase appears obvious in the coarse-grained IG, being characterized by a large number of AE events with a low initial *b* value and large increase (from ~0.5 to ~1.2, Fig. 4a, b). The intermediate-grained OG of mean grain size between WG and IG exhibits a somewhat intermediate behaviour between WG and IG, with an increasing *b* value from ~0.7 to ~1.3 (Fig. 4c, d). Such results clearly show that the temporal variation of the *b* value during the primary phase strongly depends on the grain size distribution of every test sample.

Secondary phase

The typical feature of the secondary phase is a microcracking activity in which the event rate increases, with increasing stress or time, and the *b* value decreases from its maximum at the end of the primary phase. Average values for the maximum *b* value in WG, OG, and IG are 1.4, 1.3, and 1.2, respectively (Fig. 4). Such maximum results clearly correlated with the major grain size of the test sample; a comparatively larger grain size results in a lower *b* value. In the next section, it will be shown that the energy release during the secondary phase appears to be consistent with

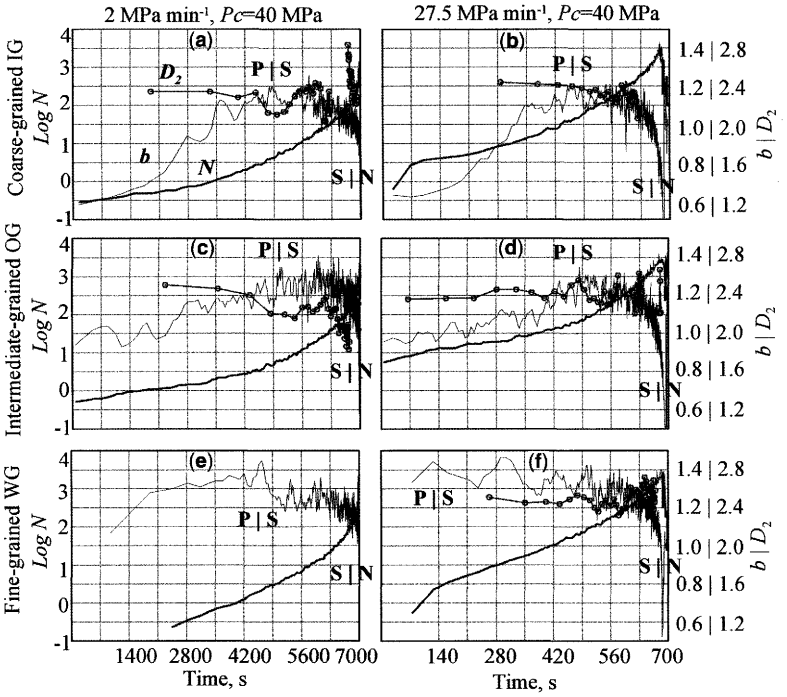

Fig. 4. The b value, fractal dimension D_2 and event rate N, obtained from tests using the IG, OG, and WG s amples under constant stress-rate loading at either 2 MPa min^{-1} or 27.5 MPa min^{-1}. 'P|S' and 'S|N' denote the transitions from the primary to the secondary and from the secondary to the nucleation, respectively. The maximum-likelihood b values were sequentially calculated for consecutive groups of 1000 events with a running step of 250 events. The fractal dimensions (D_2) were calculated for groups of 8000 events, in which the number of precisely determined hypocentres is more than 100.

a damage model based on the constitutive laws for stress corrosion applied to subcritical crack growth of crack populations.

Nucleation phase

The nucleation phase includes the nucleation and accelerated growth of failure-related features associated with the macroscopic fracture of the test sample. It is characterized by a rapidly increasing event rate, and by a rapidly decreasing b value tending to a global minimum of about 0.5.

The AE data were collected using a high-speed acoustic emission waveform recording system and applied to granitic rock samples subjected to confined compression tests; these results are summarized in Figure 5. As may be observed, the pre-failure damage evolution in these samples essentially consists of a typical three-phase pattern. In the fault zone, high AE activity was observed from the start of the test. In contrast, the AE activity began at ~95% of the strength of those samples characterized by a very low density of the pre-existing microcrack. The event rate in the GP sample of Figure 5f was very low before the final fracture, had a very short secondary phase, and a nucleation phase containing only a few foreshocks. However, more than 1000 aftershocks were recorded after the main fracture. Generally, the waveform recorder would be saturated before the final dynamic faulting. The b value in the MG, NG, and TG samples of Figure 5a–c, e increased during the primary phase from 1.0–1.2 to ~1.4.

In all cases, the transition from the primary phase to the secondary phase corresponds to the maximum b value and it can be easily determined. However, the change from the secondary phase to the nucleation phase appears to depend on the sample's grain size and on the pre-existing microscopic and macroscopic structures. When dealing with intact and homogeneous samples, the nucleation phase appears to be a natural extension of the secondary phase. Conversely, in a sample containing a macroscopic structure (Fig. 5a–c) or a very low density of pre-existing cracks (Fig. 5f), the transition occurs abruptly and coincides with the

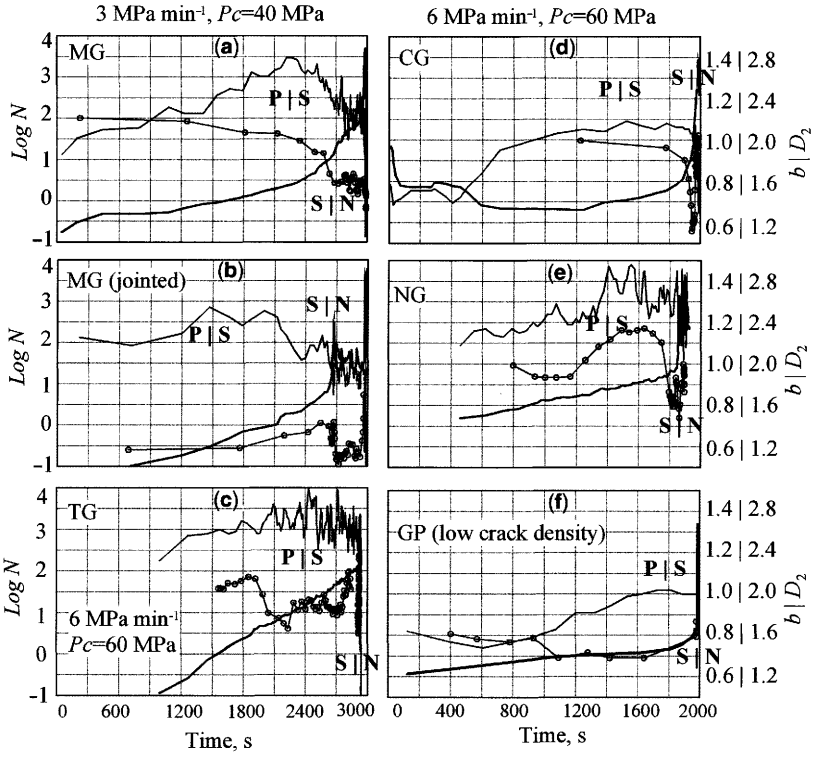

Fig. 5. The b value, fractal dimension D_2 and event rate N, obtained from rock samples under constant stress-rate loading. 'P|S' and 'S|N' denote the transitions from the primary to the secondary and from the secondary to the nucleation phases, respectively. The maximum-likelihood b values were sequentially calculated for consecutive groups of 500 events with a running step of 125 events. The fractal dimensions (D_2) were calculated for groups of 200 hypocentres.

minimum fractal dimension. The damaged fault zone rock, in sample SC, shows an abrupt onset of the nucleation phase (Fig. 5d,e). In such cases, a diffusion process of AE hypocentres, with an increasing fractal dimension, was observed during the nucleation phase (Fig. 5b–d). The time duration of the nucleation phase varies in a wide range, from a few seconds to ~100 s, and it depends first on sample lithology and pre-existing structures, and secondly on loading conditions. In general, a comparatively lower loading rate results in a longer nucleation phase, and a homogeneous sample has a comparatively shorter nucleation phase. In samples containing large-scale heterogeneous structures, such as joints or large (cm scale) grains, some short-term, large-amplitude fluctuations can be observed in the b value and in the AE rate.

Damage model

Subcritical crack growth may occur under stress as a result of stress-aided corrosion at the crack tip. The quasi-static rupture velocity V has been found experimentally to be related to the stress intensity factor K by Charles's power law (Charles 1958):

$$V = \mathrm{d}c/\mathrm{d}t = V_0(K/K_0)^l \qquad (10)$$

where V_0 is an initial/detectable velocity and K_0 is the corresponding stress intensity factor, c is the crack length (or half-crack length), and l is referred to as the stress corrosion index and has a typical value of 20–60 for polycrystalline rocks under tensile condition (Das & Scholz 1981). This power law is fundamentally based on experimental observations of mode-I crack growth of a single tensile macrocrack. It can be straightforwardly modified for a crack population having a fractal size distribution by introducing an effective mean value for each parameter (Main *et al.* 1993). However, the physical bases for such an extension have not been discussed in detail. Hereafter, c, K and V indicate the mean values of crack

length, stress intensity factor, and growth velocity, respectively.

In a generalized form, the stress intensity factor can be expressed as $K_{\mathrm{I,II,III}} = Y\sigma\sqrt{c}$, where Y is a dimensionless geometric constant and σ is the remote applied stress. Under loading conditions of constant stress rate w, $\sigma = \sigma_0 + wt$, σ_0 is the stress at $t = 0$, and the crack growth velocity can be expressed as

$$\frac{\mathrm{d}c}{\mathrm{d}t} = V_0\left(\frac{c}{c_0}\right)^{l/2}\left(\frac{\sigma}{\sigma_0}\right)^{l} = V_0\left(\frac{c}{c_0}\right)^{l/2}(1+wt)^{l}, \qquad w = \omega/\sigma_0 \tag{11}$$

where c_0 is the mean crack length at $t = 0$. The solution of the above differential equation under the initial condition $c = c_0$ at $t = 0$, is

$$c = c_0\left(1 - \frac{(l-2)v_0((1+wt)^{l+1}-1)}{2w(l+1)c_0}\right)^{2/(2-l)}, \quad w \neq 0$$
$$c = c_0\left(1 - \frac{(l-2)v_0}{2c_0}t\right)^{2/(2-l)}, \quad w = 0. \tag{12}$$

The mean crack length c increases nonlinearly with time. A failure time can be defined as t_{f} so that c approaches infinity:

$$t_{\mathrm{f}}(w) = \frac{1}{w}\left(\left(\frac{2w(l+1)c_0}{(l-2)v_0}+1\right)^{1/(l+1)} - 1\right), \; w \neq 0$$
$$t_{\mathrm{f}} = \frac{2c_0}{(l-2)v_0}, \; w = 0. \tag{13}$$

Under constant stress ($w = 0$), Eq. (13) reduces to the same equation given by Das & Scholz (1981). Equation (12) can be simplified as

$$c \approx c_0(1 - t/t_{\mathrm{f}}(w))^{2/2-l}, \; w \neq 0$$
$$c = c_0(1 - t/t_{\mathrm{f}})^{2/2-l}, \; w = 0. \tag{14}$$

Under constant stress-rate loading Eq. (14) is a good approximation of the exact solution (12). Equation (14) can be further simplified by using the normalized time-to-failure defined in Eq. (1):

$$c = c_0\tilde{t}^{2/2-l}, \; \tilde{t} > 0. \tag{15}$$

This is again a power law. Meredith & Atkinson (1983) showed experimentally that the event rate N of the microcrack activity during the subcritical crack growth of a single tensile crack also exhibits a nonlinear dependence on the stress intensity, showing a form similar to Charles's power law:

$$N = N_0(K/K_0)^{l'}. \tag{16}$$

Within this context, l' is referred to as the 'effective' stress corrosion index and is found to be equal to n within a few percent in brittle rocks (Main & Meredith 1991). From Eq. (16), the event rate can be represented by

$$N = (1 - t/t_{\mathrm{f}})^{2l'/2-l}(1+wt)^{l'}. \tag{17}$$

This model is roughly representative of the AE data in granitic samples under differential compression (Lei *et al.* 2005). However, the fit of the results typically shows $l' = 12$ and $l = 25$–45. We note that l' is only a half to a third of l. This is most likely because l is excessively high for compression tests due to the occurrence of mixed fracture models. Generally, a shear crack should be more stable than a tensile crack. For modelling purposes, it is better to refer to energy release rather than event rate.

Under differential compression, the observable data are the magnitude and the hypocentre of the AE events. Thus, a model ought to be derived for the release rate of energy, instead of the increment of crack length. It was found both observationally and theoretically (Kanamori & Anderson 1975) that there is a power-law scaling relation between the release of elastic energy and the rupture area (S):

$$E = 10^{1.5M_i} \propto S^{3/2}; \tag{18}$$

hence, the increase rates of fracture area can be estimated from AE data by

$$\dot{S}_{\mathrm{AE}}(t)/\dot{S}_{\mathrm{AE}}(0) = \sum\left(10^{1.5M_i}\right)^{2/3} = \sum 10^{1.0M_i} \tag{19}$$

where the sums are over all events in an individual period of unit time at the given time t. It should be mentioned that Eq. (19) provides an underestimate, because of increasing energy loss with the increase of the mean crack length from the AE source through the receiver. The major factors associated with such loss include (1) frictional heat, (2) scattering of elastic waves through a damaged volume, and (3) progressive replacement of tensile cracking by shear cracking. The total effect of all these factors is assumed to be a function of the mean

crack length c in terms of a power law:

$$\dot{S}_{AE} = \dot{S}c^{-m} = 2\dot{c}c^{1-m}, \qquad m \geq 0. \tag{20}$$

Therefore, the basic equation for modelling the AE data can be expressed by

$$E_1(t)/E_1(0) = (1 - t/t_f)^{l+2-2m/2-l}(1 + wt)^l. \tag{21}$$

Here, $E_1 = \sum 10^{1.0M_i}$ indicates the energy release rate evaluated by the measured AE magnitude.

The fit of Eq. (21) to AE data obtained by typical experiments is shown in Figure 6. As a general rule, except for the primary phase ($\tilde{t} > 1$), AE energy release data can be well represented by the aforementioned model. The best parameters, which match the AE data, are $m = 2.4$–3.6 and $l = 8$–16, depending on the grain size and lithological type. Such values of l are significantly lower than the typical value of 25–45 obtained by using Eq. (16) for the event rate, and appear more reasonable. The fine-grained samples have smaller m and larger l values ($m = 3.0$, $l = 16$) than coarse-grained samples ($m = 3.6$, $l = 12$), whereas westerly granite displays smaller m and l ($m = 2.8$, $l = 8$–10). It is obvious that both m and l are independent of the loading rates.

The first term in Eq. (21), which governs the nonlinear acceleration of damage, can be ignored when $t \ll t_f$. However, it dominates when t approaches t_f. It is clear that if a rock sample contains some pre-existing macroscopic cracks or joints, which can potentially serve as the ultimate fracture plane, the overall deformation behaviour of the material could be governed by such cracks, following their initiation, as a result of high nonlinearity in the model. In such cases, the damage model is basically

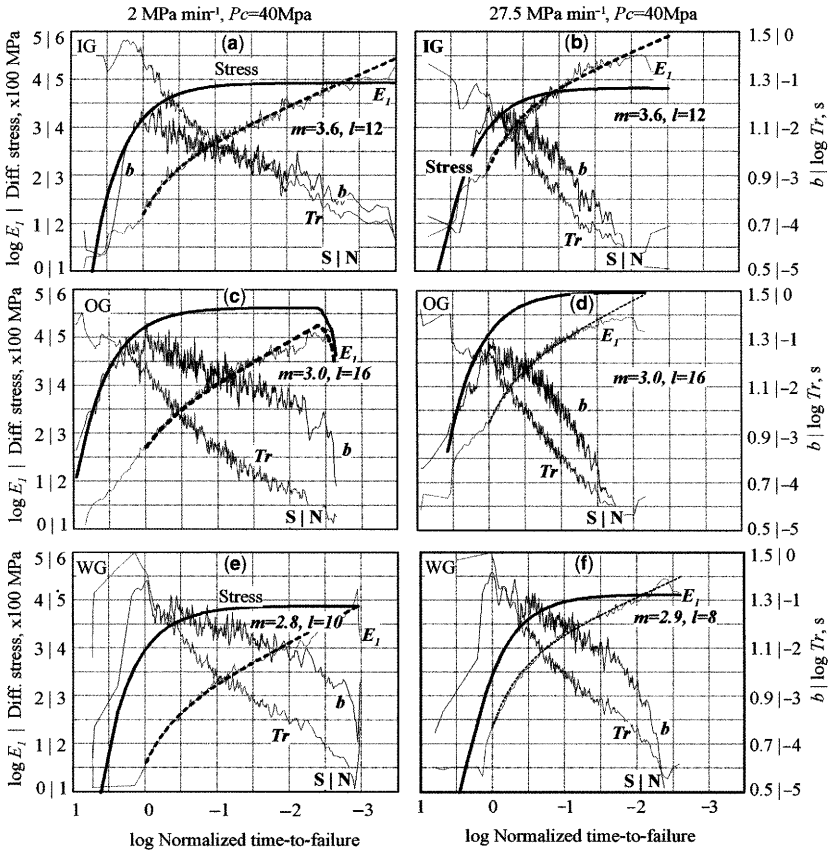

Fig. 6. Key AE data of three granites (IG, OG, WG) having different grain size distribution, under two loading rates of 2.0 and 27.5 MPa min^{-1}. The time axis corresponds to the normalized time-to-failure on a log scale, for presenting the acceleration of the evolution of the pre-failure damage. The dashed lines indicate the fit of the results of the subcritical crack growth model with the energy release rate (E_1). 'P|S' and 'S|N' denote the transitions from the primary to the secondary and from the secondary to the nucleation, respectively.

applicable. However, the observed data cannot be represented by a single fit. It should be mentioned that for a small value of loading rate w including creep test ($w = 0$), neither m nor l can be determined because, for any given constant F, relation (21) gives similar results for every set of (m, l) satisfying $m = [(1 + F)l + 2(1 - F)]/2$. However, m and l can be determined from AE data obtained from tests with a loading rate efficiently larger than zero.

In addition, the relative stress intensity factor can be estimated from the AE release rate as

$$\frac{K}{K_0} = (E_1(t)/E_1(0))^{1/l+2(1-m)}. \quad (22)$$

Meredith & Atkinson (1983) showed that the seismic b value is in fact negatively correlated with the stress intensity K normalized by the fracture toughness K_c. Because K/K_0 can be estimated from Eq. (22), the correlation of b and K can be expressed alternatively as

$$b = b_0 - a(K/K_0). \quad (23)$$

Figure 7 shows the maximum-likelihood b values against the normalized stress intensity factor estimated by Eq. (22) in fine-grained and in coarse-grained samples both under fast (27.5 MPa min^{-1}) and low (2 MPa min^{-1}) stress rates. The experimental data basically fit the linear correlation defined by Eq. (23); however, data with b values less than 0.8 are systematically not represented by a linear trend. Such scattered data coincide with the last stage, immediately preceding the catastrophic failure. During this stage, larger and larger events frequently occur. A great number of events are embedded within the tail of the previous event. Moreover, events of amplitude larger than 100 dB were clipped and recorded as an event of a relative magnitude of 2.75. As a result, both the b value and K/K_0 are likely to be underestimated during the last stage.

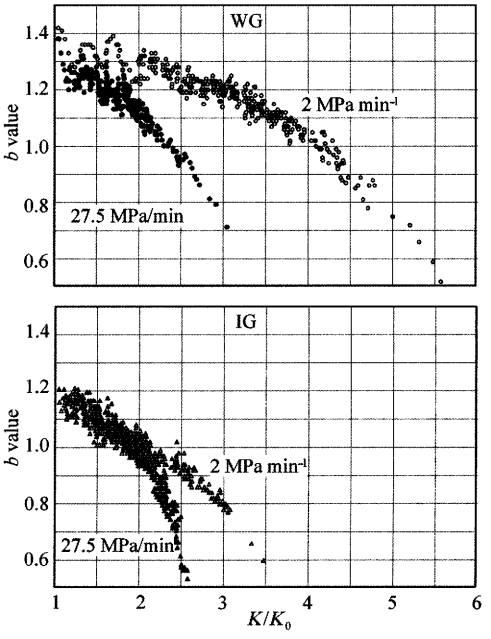

Fig. 7. For two granitic samples WG and IG, the maximum likelihood b values during the secondary and nucleation phases plotted v. K/K_0 estimated from the AE energy release rate. Note that K_0 at time t_0 corresponds to the start of the secondary phase, or in other words, the start of the subcritical crack growth.

Discussion

Fracture mechanism of the primary damage phase

It is clearly recognized that every damage phase is governed by somewhat different fracture mechanisms and that the statistical behaviour of every typical phase strongly depends on the density and size distribution of pre-existing microcracks, which are controlled by grain size distribution within the test sample. The damage model and its fit to experimental data provided some strong insights into the pre-failure damage process in the brittle domain.

Based on experimental results, it appears reasonable to assume that the major mechanism of microcracking in the primary phase is associated with some kind of initial rupture of pre-existing flaws. The primary phase shows behaviours that cannot be represented by the damage model based on subcritical crack growth of crack populations. This supports the hypothesis that microcracking during the primary phase is related to the initial rupture of the pre-existing flaws, rather than to subcritical crack growth. The pre-existing microcracks are probably healed prior to loading, and consequently the initial rupture proceeds more easily by separating the crack walls rather than by crack growth. Because a number of mechanisms can originate local tensile stress, and because the extension strength of every crack is much lower than shear strength, it follows that microcrack opening is expected to be the predominant cracking mode during the primary phase. It can be well understood that the primary phase shows an increasing b value with increasing stress, because larger pre-existing microcracks have a higher probability of rupturing at comparatively lower stress.

As shown in Figures 4 and 5, the event number during the primary phase decreases significantly. In addition, the fractal dimension of the hypocentres showed no significant stress dependence. Compared to smaller grain sizes, the comparatively larger grain size samples show a lower initial b, a larger maximum b, and a lower D_2. As the distribution of pre-existing microcracks is controlled by grain size distribution, it is observed that (1) the larger mean grain sizes correspond to a larger number of large cracks and (2) the event rates, the b values, and the fractal dimensions all appear to be consistent with the hypothesis that the primary phase is associated with the initial activity of pre-existing cracks. Therefore, during the primary phase, the b value and fractal dimension reflect the size distribution and spatial distribution of pre-existing microcracks, respectively. Although both parameters appear to depend on grain size distribution of the test sample, no intrinsic correlation was observed between them.

Fracture mechanism of the secondary and nucleation damage phases

The damage model illustrated above represents appropriately the AE energy release rate during the secondary and nucleation phases. This implies that the fracture laws governing the mode-I microcracking during a single extensional growth of a macrocrack, also control the mixed mode of microcracking activity under differential compression. Although the brittle behaviour of rocks under compression is complex, it is clear that on a grain or microcrack scale, a variety of mechanisms give rise to localized tensile stress. The formation and growth of shear faults in a very fine-grained rock under triaxial compression is therefore guided by the development of a process zone encompassing tensile microcracks at the fault tip (Lei *et al.* 2000*b*). Under differential compression, many AE events also show a nonquadrantal distribution of the P first motions, hence suggesting that they may record the growth of typical wing cracks, that is, a shear cracks with tensile tails (Lei *et al.* 2000*b*). Other possible mechanisms causing local tensile stress are:

(1) contacts between grains;
(2) bending of elongated grains; and
(3) indentation of sharp-cornered grains into neighbouring ones.

As a result, independently of the remote applied stress, mode-I tensile cracking is likely to be the major mechanism for creating a new crack surface and for contributing to subcritical crack growth. Furthermore this common micro-mechanism provides a possible physical base for justifying why fracture laws derived from extension tests of single macroscopic cracks can also be used for representing the statistical behaviour of mixed-mode crack populations. The fact that the proposed model represents very well the AE energy release rate during the secondary and nucleation phases also supports the assumption that the damaging process involves mainly the subcritical growth of pre-existing microcracks. Following increase of the mean crack length, the energy release rate increases nonlinearly, while the b value decreases almost linearly with the normalized mean stress intensity factor, which was estimated by the AE release data.

The nucleation phase is characterized by a progressively increasing release rate and by a rapidly decreasing b value, which ultimately reaches a global minimum of 0.5. This is the most interesting and important phase during the catastrophic fracture of rock samples that contain heterogeneous faults. The term 'nucleation' is used here rather than 'tertiary phase' because it better describes the nucleation process of the ultimate, unstable fracture. Once the final fault is initiated at one or at several key locations, which could be the edges of asperities or of previously fractured areas, the faulting process will be governed by the accelerating growth of a few very large cracks, or by the progressive fracture of the major asperities on the fault surface.

The proposed damage model, when applied to the nucleation phase, emphasizes that the data fit is not satisfactory, due to the governing behaviour of a few large cracks. Following the increase of the mean crack length of the crack population, interaction between cracks becomes in fact more and more important. This interaction results in fluctuations of both the energy release and b value; consequently, macroscopic heterogeneity, such as pre-existing joints or asperities on the final fracture surface, have a strong influence on the damage evolution of the nucleation phase. As already mentioned, the duration time of the nucleation phase varies in a wide range, from a few seconds to $\sim$100 s, depending on the density of the pre-existing microcracks as well as the loading rate of stress. For any given lithology containing a fault with unbroken asperities, a creep test at constant stress would show a comparatively longer nucleation phase than that recorded at constant stress-rate load (Lei 2003).

Summarizing the main findings of the nucleation phase, it may therefore be emphasized that (1) this phase records the quasi-static nucleation of the final fault; (2) the damaging process is associated with the progressive fracture of several unbroken asperities on the fault surface; and (3) the AE events caused by the fracture of individual

asperities exhibit similar characteristics to those of natural earthquakes, including foreshock, mainshock, and aftershock events. The foreshocks, which initiated at the edge of the asperity, occur with an event rate that increases according to a power law of the temporal distance to the mainshock, and with a decreasing b value (from ~1.1 to ~0.5). One or a few mainshocks are then initiated at the edge of the asperity or at the front of the foreshocks. The aftershock period is characterized by a remarkable increase and subsequent gradual decrease in the b value, and by a decreasing event rate, thus obeying the modified Omori law, which has been well established for earthquakes. The fracture of neighbouring asperities is initiated after a mainshock associated to a specific asperity, presumably due to redistribution of the strain energy. The entire process results therefore in the enhancement of stress concentration around the nearest neighbouring intact asperities. The progressive fracturing of multiple, coupled asperities results in some short-term precursory fluctuations both in the b value and in the event rate. However, it is believed that at constant stress-rate loading conditions, this kind of process could be accelerated dramatically.

The significance of the b *value*

Since the 1960s, b-value variations have been directly related to the local stress conditions (Scholz 1968). In the present study, great efforts have been devoted towards investigating the physical significance of the b value in the magnitude–frequency relation, and it as been shown that, in fact, the state of stress plays the most important role in determining the value of b, which is well represented by a linear relation with the stress intensity factor (Fig. 7). However, the present study also shows that, at a given stress condition, the b values strongly depend also on rock heterogeneity, as this is a major factor governing pre-failure damage and fracture dynamics. However, the concept of heterogeneity is somewhat scale-dependent. With regard to sample size, for example, the greatest grain size can be considered as an index of rock heterogeneity. However, for every microcrack, because its size is generally less than the greatest grain, a sample with a comparatively smaller grain may show greater heterogeneity.

In general, available experimental data clearly show that the b value, in every phase, obeys the general relationship: $b_{IG} < b_{OG} < b_{WG}$, hence suggesting that a comparatively larger grain size results in a lower b value. Furthermore, experimental data show that b values may vary, depending on stress, between 0.5 and 1.5, and that fault zone rocks have a comparatively smaller b value than its host rock of the same lithology (Fig. 5d, e). On the other hand, samples with low pre-existing crack density also have significantly lower b values than those with high pre-existing crack density (Fig. 5f). Finally, both experiments and numerical simulations show that the b value of AE events is controlled by variations of the internal friction angle, which are induced by variations in confining pressure (Amitrano 2003).

In conclusion, the b value can be considered a good parameter for measuring the capability of rocks to release accumulated strain energy. With this aim, possible correlations between the b value and crack interaction, as well as assessment of the dependence of the b value on fracture mechanisms, may represent major items for future studies.

Damage localization and failure nucleation

It has been shown that the AE hypocentre distribution shows complicated clustering behaviours during the pre-damage evolution. Nevertheless, as shown in Figure 8, there are several common features that may be of interest:

(1) In coarse-grained samples, grain size has the role of characteristic scale, leading to a band-limited fractal or bifractal structure. Large bands (L) and small bands (S) may

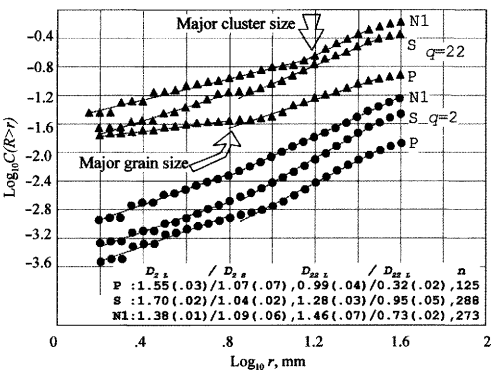

Fig. 8. Generalized correlation integral of the AE hypocentres in coarse-grained and jointed samples. Note that the AE hypocentre exhibits some heterogeneous fractal and bifractal structures; the fractal dimensions estimated for large bands (L) and small bands (S), at $q = 2$ and 22 are also shown. The numbers in parenthesis are estimation errors. P and S indicate the primary and secondary phases, respectively. N1 indicates the earlier stage of the nucleation phase. The number n indicates the number of hypocentres used for the calculation of the correlation integral.

likely show different fractal dimensions. However, in fine-grained samples, this kind of characteristic scale could not be found, possibly because it is smaller than the available precision of hypocentre determination.

(2) AE hypocentre distribution exhibits multifractal features, with changing values of D_2-D_{22}, indicating heterogeneity changes during damage evolution (Fig. 8).

(3) Damage localization associated with the growth of a fault is characterized by minimum D values measured at the onset of the nucleation phase (Fig. 4c, Fig. 5a–e).

The final phase of damage evolution is of outstanding interest for short-term prediction of catastrophic fracture development. However, the transition from the secondary to the nucleation phase is strongly affected by the homogeneity of the test sample. In samples containing one or more pre-existing joints, a strong localization was observed along some discontinuities that were ultimately ruptured (Fig. 9; see also Satoh *et al.* 1996). Clear damage localization was also observed in samples with a few large (cm scale) grains, where the final rupture was mostly controlled by the grain boundaries of some large grains. Samples with high pre-existing crack density, such as the foliated granitic cataclasite from the Nojima fault zone, show less brittle behaviour and a gradual damage localization followed by clear diffusion. This results in a significant decrease and subsequent increase in fractal dimension (Fig. 5d).

In the case of intact rocks, loaded at a constant stress rate, during the final stage the microcracking occurred so frequently that it was impossible to distinguish every event from the AE waveforms. Hence, it was impossible to clarify the damage localization on the basis of the AE hypocentre distribution. By using the event rate as a feedback signal to control the loading system, the nucleation phase, which would otherwise have taken only a few seconds, could be extended to several hours duration, and the quasi-static nucleation could be mapped using the AE hypocentres (see also Lockner *et al.* 1991). In addition, the faulting nucleation could be controlled by using an asymmetrical loading cell (Zang *et al.* 2000) and the result was a final shear fracture, initiated from some artificially determined point, at a relatively lower stress level and lower AE background. In such cases, the damage localization was clearly established.

Relationship between the b *value and the fractal dimension*

In a fractal fault system, the fractal dimension (D_S) of the distribution of fault length is correlated with the b value of earthquakes:

$$D_S = 2b. \tag{24}$$

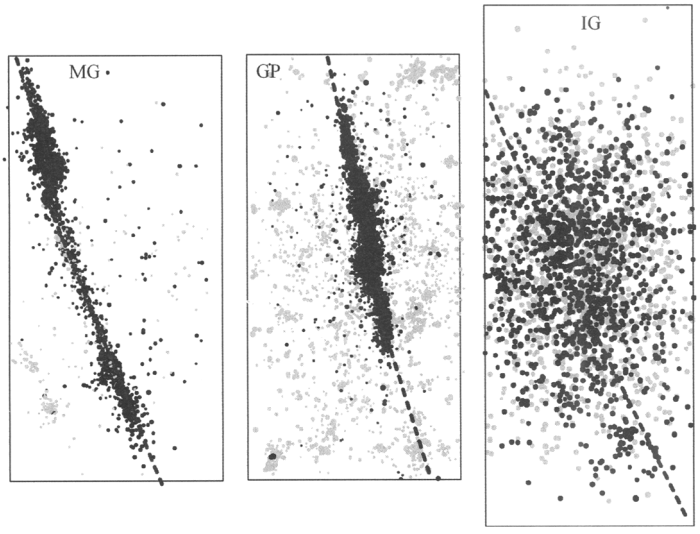

Fig. 9. AE hypocentres in three coarse-grained granites. AE hypocentres during the pre-nucleation (grey circles) and nucleation (black circles) phases. A clear localization of the damage was observed in two samples only. During the nucleation phase, the AE rate was so high that most events occurred on a very noisy background, and it was difficult to determine a sufficient number of P arrival times for hypocentre determination; as a result, the damage localization could not be identified.

This result derives from the interrelationships between the frequency–magnitude (Gutenberg & Richter 1944), moment–magnitude (Aki 1967), and moment–source area (Kanamori & Anderson 1975). It would be interesting also to establish whether a similar correlation exists between (1) the b value and the fractal dimension of the spatial distribution of earthquake hypocentres, or (2) the fractal dimension and the spatial distribution of active faults (see also Cello *et al.* 2006, this volume). Regarding point (1), the AE data by Lockner *et al.* (1991) show that a decrease of the b value appears to be correlated, with no time shift, with strain localization, that is, with a decrease of the D value. Regarding point (2), both positive and negative correlations are reported (e.g. Oncel *et al.* 2001). The present study furnishes some additional information on this critical problem, as it has been observed that, during the primary phase, the b value increased with increasing stress, but the fractal AE hypocentre dimension did not show any systematic variation. The b value and fractal dimension reflect, in fact, the size distribution and spatial distribution of pre-existing microcracks, respectively. In other words, there is no intrinsic correlation between the b value and fractal dimension.

However, as already mentioned, in some cases, well-defined damage localization and subsequent damage diffusion were observed while evolving from the secondary to the nucleation phases. The change from decreasing to increasing fractal dimension corresponds to the onset of the nucleation phase. However, during the localization–diffusion process, the b value as a long-term average exhibits a monotonous decrease until the final dynamic fracturing. As a result, a positive correlation between b and D_2 was observed during the localization stage, while a negative correlation was observed during the diffusion stage. Figure 10 shows the fractal dimension D_2 against the b values obtained from the tests shown in Figures 4 and 5.

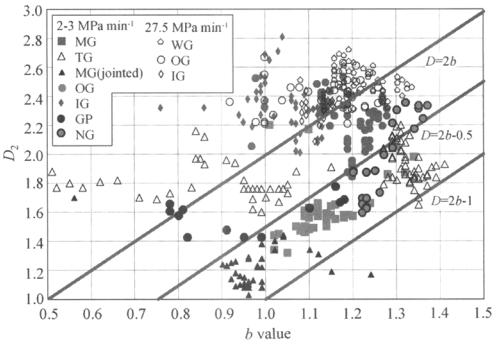

Fig. 10. The fractal dimension D_2 of AE hypocentres v. the b value obtained from the tests shown in Figures 4 and 5. In some cases, D_2 correlates linearly with b as $D_2 = 2b + constant$ (see text for details).

Predictability of rock failure

The experimental results indicate that, either the accelerated energy release rate or the decreasing b value can be used to predict the final catastrophic event successfully. However, for the natural cases, particularly for the prediction of large earthquakes, the situation appears to be much more difficult. First, because large earthquakes are normally nucleated at depths of between a few km and tens of km, it is impossible to obtain sufficient information from the surface-based seismic monitoring networks. Secondly, most large earthquakes occur along well-developed active faults, and are governed by some kind of mixed mechanism including frictional sliding on the fault surface and rock fracture. In spite of this, some precursory phenomena are known to appear months and even years before large earthquakes and volcanic eruptions occur (e.g. Imoto 1991; Hurukawa 1998; Vinciguerra 1999; Zuniga & Wyss 2001; Nuannin *et al.* 2005).

The proposed three-phase damage model may therefore be profitably used for interpreting the sequence of phases preceding catastrophic failure events, including natural processes such as volcanic eruptions, mining-induced rock bursts, and earthquakes. The decrease of the b value and the onset of the nucleation phase, which generally corresponds to the minimum value of the fractal dimension of hypocentres, are key indicators of the preparatory stage of a catastrophic event.

More generally, short-term prediction depends on reliable precursory phenomena. A reliable precursor should follow well-defined empirical laws, and should be related to some plausible physical mechanism. Experimental approaches under well-controlled conditions are considered useful for finding possible precursors and their related physical mechanism. To this aim, the present study clearly shows that a comparatively greater heterogeneity results in a longer and more complicated nucleation phase, with a larger number and more types of precursory anomalies. Differently stated, the catastrophic failure event can be better predicted in a comparatively more heterogeneous rock mass. It is expected that the interaction between neighbouring cracks becomes increasingly significant as a result of the progressive increase of both density and length of every crack. In heterogeneous rocks, such as in coarse-grained granites, the interactions are markedly affected by the heterogeneous structure, thus causing fluctuations with large amplitude

in the damage statistics. Such a strong dependence of pre-failure damage on local structure indicates that the predictability of catastrophic events is also site-dependent. Pre-failure damage evolution likely varies greatly in each case; hence, it is particularly important to resolve, for a given target site, the local geological structure. Systematic studies on the simulation of various geological structures are in fact meaningful for prediction purposes. Future studies need therefore to be focused on establishing quantitative correlations between fluctuations of energy release and the heterogeneous structure of the crust.

Conclusions

AE data from granitic rock samples indicate that the pre-failure damage process is characterized by three typical phases of microcracking activity: the primary, secondary, and nucleation phases. It was assessed that the evolution of the three-phase pre-failure damage is a common feature within granitic lithologies having different grain size distributions, as well as macrostructures such as joints. The primary phase reflects the initial opening or ruptures of pre-existing microcracks, and it is characterized by an increase, with increasing stress, both of the event rate and the b value. The secondary phase involves the subcritical growth of the microcrack population, revealed by an increase, with increasing stress, in the energy release rate and a decrease in the b value. The nucleation phase corresponds to the initiation and accelerated growth of the ultimate fracture along either one or several incipient fracture planes. During the nucleation phase, the b value decreases rapidly down to the global minimum value of 0.5.

Beside the experimental study, a theoretical analysis was performed, in order to improve the damage model based on the constitutive laws of subcritical crack growth for crack populations whose size distribution is fractal. Instead of modelling the event rate as in some earlier studies, the energy release rate was fitted by using this improved model. The model can represent very well the AE energy release rate in three granites of different grain size distribution, implying that the fracture laws (the same laws as those in mode-I microcracking during a single extensional growth of a macrocrack) actually governed the mixed mode of the microcracking activity under differential compression.

The fractal dimension of the AE hypocentres appears also to be consistent with the fracture mechanisms peculiar of every phase. During the primary phase, the fractal dimension depends on grain size and it shows no significant temporary variation. Hence it reflects the spatial distribution of pre-existing cracks. Some more or less pronounced decrease of the fractal dimension was observed, being associated with the rapid decrease of the b value. The fractal dimension decreased down to a minimum value around the onset of the nucleation phase. A diffusion process of AE hypocentres was also observed, in some cases, following the onset of the nucleation phase. The progressive development of the fracturing through heterogeneous rocks of large grain size, and through samples that include macroscopically heterogeneous structures such as joints, results in some short-term precursory fluctuations, both in the b value and in the energy release rate.

The results of this study indicate that the precursor-based predictability of catastrophic failure is highly dependent on pre-existing heterogeneity and loading conditions. The most important factors are the density and size distributions of pre-existing cracks. The three-phase model proposed in this study appears to be meaningful for transferring the experimental results to real situations associated with both artificial applications and natural processes affecting crustal rocks.

This research was supported by the Japan Society for the Promotion of Science under grant 14340128, the Ministry of Science and Technology of China under grant 2004BA601B01 and the National Natural Science Foundation of China under grant 40127002. Helpful reviews by G. P. Gregori and F. Storti are gratefully acknowledged. I would also like to express my gratitude to G. Cello for his helpful comments and suggestions.

References

AKI, K. 1965. Maximum likelihood estimate of b in the formula $\log N = a - bm$ and its confidence. *Bulletin of Earthquake Research Institute, University Tokyo*, **43**, 237–239.

AKI, K. 1967. Scaling law of seismic spectrum. *Journal of Geophysical Research*, **72**, 1217–1231.

AMITRANO, D. 2003. Brittle–ductile transition and associated seismicity: Experimental and numerical studies and relationship with the b value. *Journal of Geophysical Research*, **108(B1)**, 2044, doi:10.1029/2001JB000680.

BENDER, B. 1983. Maximum likelihood estimation of b values for magnitude grouped data. *Bulletin of the Seismological Society of America*, **73**, 831–851.

CHARLES, R. J. 1958. Static fatigue of glass. *Journal of Applied Physics*, **29**, 1549–1560.

COX, S. J. D. & SCHOLZ, C. H. 1988. Rupture initiation in shear fracture of rocks: an experimental study. *Journal of Geophysical Research*, **93(B4)**, 3307–3320.

DAS, S. & SCHOLZ, C. H. 1981. Theory of time-dependent rupture in the Earth. *Journal of Geophysical Research*, **86**, 6039–6051.

DIEDERICHS, M. S., KAISER, P. K. & EBERHARDT, E. 2004. Damage initiation and propagation in hard rock during tunnelling and the influence of near-face stress rotation. *International Journal of Rock Mechanics and Mining Sciences*, **41**, 785–812.

DIODATI, P., BAK, P. & MARCHESONI, F. 2000. Acoustic emission at the Stromboli volcano: scaling laws and seismic activity. *Earth and Planetary Science Letters*, **182**, 253–258.

GUTENBERG, B. & RICHTER, C. F. 1944. Frequency of earthquakes in California. *Bulletin of the Seismological Society of America*, **34**, 185–188.

HURUKAWA, N. 1998. The 1995 off-Etorofu earthquake: joint relocation of foreshocks, the mainshock, and aftershock and implications for the earthquake nucleation process. *Bulletin of the Seismological Society of America*, **88**, 1112–1126.

IMOTO, M. 1991. Changes in the magnitude-frequency *b*-value prior to large ($M \geq 6.0$) earthquakes in Japan. *Tectonophysics*, **193**, 311–325.

JOUNIAUX, L., MASUDA, K., LEI, X.-L., NISHIZAWA, O., KUSUNOSE, K., LIU, L. & MA, W. 2001. Comparison of the microfracture localization in granite between fracturation and slip of a pre-existing macroscopic healed joint by acoustic emission measurements. *Journal of Geophysical Research*, **106(B5)**, 8687–8698.

KANAMORI, H. & ANDERSON, D. L. 1975. Theoretical basis of some empirical relations in seismology. *Bulletin of the Seismological Society of America*, **65**, 1073–1095.

KURTHS, J. & HERZEL, H. 1987. An attractor in a solar time series. *Physica*, **25D**, 165–172.

LEI, X.-L. 2003. How do asperities fracture? An experimental study of unbroken asperities. *Earth and Planetary Science Letters*, **213**, 345–357.

LEI, X.-L., NISHIZAWA, O., KUSUNOSE, K. & SATOH, T. 1992. Fractal structure of the hypocenter distribution and focal mechanism solutions of AE in two granites of different grain size. *Journal of Physics of the Earth*, **40**, 617–634.

LEI, X.-L., NISHIZAWA, O. & KUSUNOSE, K. 1993. Band-limited heterogeneous fractal structure of earthquakes and acoustic-emission events. *International Geophysical Journal*, **115**, 79–84.

LEI, X.-L., KUSUNOSE, K., NISHIZAWA, O., CHO, A. & SATOH, T. 2000*a*. On the spatio-temporal distribution of acoustic emission in two granitic rocks under triaxial compression: the role of pre-existing cracks. *Geophysical Research Letters*, **27**, 1997–2000.

LEI, X.-L., KUSUNOSE, K., RAO, M. V. M. S., NISHIZAWA, O. & SATOH, T. 2000*b*. Quasi-static fault growth and cracking in homogeneous brittle rock under triaxial compression using acoustic emission monitoring. *Journal of Geophysical Research*, **105(B3)**, 6127–6140.

LEI, X.-L., NISHIZAWA, O., KUSUNOSE, K., CHO, A. & SATOH, T. 2000*c*. On the compressive failure of shale samples containing quartz-healed joints using rapid AE monitoring: the role of asperities. *Tectonophysics*, **328**, 329–340.

LEI, X.-L., KUSUNOSE, K., SATOH, T. & NISHIZAWA, O. 2003. The hierarchical rupture process of a fault: an experimental study. *Physics of the Earth and Planetary Interior*, **137**, 213–228.

LEI, X.-L., MASUDA, K. *ET AL.* 2004. Detailed analysis of acoustic emission activity during catastrophic fracture of faults in rock. *Journal of Structural Geology*, **26**, 247–258.

LEI, X.-L., SATOH, T., NISHIZAWA, O., KUSUNOSE, K. & RAO, M. V. M. S. 2005. Modelling Damage Creation in Stressed Brittle Rocks by Means of Acoustic Emission. *Proceedings of 6th International Symposium on Rockbursts and Seismicity in Mines (RsSim6)*, Perth, Australia, 327–334.

LIAKOPOVLOU-MORRIS, F., MAIN, I. G. & CRAWFORD, B. R. 1994. Microseismic properties of a homogeneous sandstone during fault nucleation and frictional sliding. *International Geophysical Journal*, **119**, 219–230.

LIN, A. 2001. S-C fabrics developed in cataclasitic rocks from the Nojima fault zone, Japan and their implications for tectonic history. *Journal of Structural Geology*, **23**, 1167–1178.

LOCKNER, D. A., BYERLEE, J. D., KUKSENKO, V., PONOMAREV, A. & SIDORIN, A. 1991. Quasi-static fault growth and shear fracture energy in granite. *Nature*, **350**, 39–42.

MAIN, I. G. & MEREDITH, P. G. 1991. Stress corrosion constitute law as a possible mechanism of intermediate-term and short-term seismic quiescence. *International Geophysical Journal*, **107**, 363–372.

MAIN, I. G., MEREDITH, P. G. & JONES, C. 1989. A reinterpretation of the precursory seismic *b* value anomaly from fracture mechanics. *Geophysical Journal*, **96**, 131–138.

MAIN, I. G., SAMMONDS, P. R. & MEREDITH, P. G. 1993. Application of a modified Griffith criterion to the evolution of fractal damage during compressional rock failure. *International Geophysical Journal*, **115**, 367–380.

MEREDITH, P. G. & ATKINSON, B. K. 1983. Stress corrosion and acoustic emission during tensile crack propagation in Whin Sill dolerite and other basic rocks. *Geophysical Journal of the Royal Astronomical Society*, **75**, 1–21.

NUANNIN, P., KULHANEK, O. & PERSSON, L. 2005. Spatial and temporal b value anomalies preceding the devastating off coast of NW Sumatra earthquake of December 26, 2004. *Geophysical Research Letters*, **32**, L11307, doi:10.1029/2005GL022679.

ONCEL, A. O., WILSON, T. H. & NISHIZAWA, O. 2001. Size scaling relationship in the active fault networks of Japan and their correlation with Gutenberg–Richter b values. *Journal of Geophysical Research*, **106(B10)**, 21827–21841.

PONOMAREV, A. V., ZAVYALOV, A. D., SMIRNOV, V. B. & LOCKNER, D. A. 1997. Physical modelling of the formation and evolution of seismically active fault zones. *Tectonophysics*, **277**, 57–81.

SATOH, T., SHIVAKUMAR, K., NISHIZAWA, O. & KUSUNOSE, K. 1996. Precursory localization and development of microfractures along the ultimate fracture plane in amphibolite under triaxial creep. *Geophysical Research Letters*, **23**, 865–868.

SCHOLZ, C. H. 1968. The frequency–magnitude relation of microcracking in rock and its relation to earthquakes. *Bulletin of the Seismological Society of America*, **58**, 399–415.

SHI, Y. & BOLT, B. A. 1982. The standard error of the magnitude-frequency *b* value. *Bulletin of the Seismological Society of America*, **72**, 1677–1687.

SUN, X., HARDY, H. R. & RAO, M. V. M. S. 1991. Acoustic emission monitoring and analysis procedures utilized during deformation studies on geologic materials. *In*: SACHSE, W., ROGET, J. & YAMAGUCHI, K. (eds) *Acoustic Emission: Current Practice and Future Directions*. ASTM Special Technical Publication, 365–380.

TAPPONIER, P. & BRACE, W.F. 1976. Development of stress induced microcracks in Westerly granite. *International Journal of Rock Mechanics and Mining Science Abstracts*, **13**, 103–112.

VINCIGUERRA, S. 1999. Seismic scaling exponents as a tool in detecting stress corrosion crack growth leading to the September–October 1989 flank eruption at Mt. Etna volcano. *Geophysical Research Letters*, **26**, 3689–3692.

UTSU, T. 1965. A method for determining the value of *b* in a formula log $n = a - bm$ showing the magnitude–frequency relation for earthquakes (in Japanese). *Geophysical Bulletin*, **13**, 99–103.

WEISS, J. 1997. The role of attenuation on acoustic emission amplitude distributions and b-values. *Bulletin of the Seismological Society of America*, **87**, 1362–1367.

ZANG, A., WAGNER, F. C., STANCHITS, S., JANSSEN, C. & DRESEN, G. 2000. Fracture process zone in granite. *Journal of Geophysical Research*, **105(B10)**, 23651–23661.

ZHAO, Y. 1998. Crack pattern evolution and a fractal damage constitutive model for rock. *International Journal of Rock Mechanics and Mining Science*, **35**, 349–366.

ZUNIGA, F. R. & WYSS, M. 2001. Most- and least-likely locations of large to great earthquakes along the Pacific coast of Mexico estimated from local recurrence time based on b-values. *Bulletin of the Seismological Society of America*, **91**, 1717–1728.